



City Research Online

City St George's, University of London

Citation: Themistos, C., Rajarajan, M., Rahman, B. M. & Grattan, K. T. V. (2009). Characterization of Silica Nanowires for Optical Sensing. *Journal of Lightwave Technology*, 27(24), pp. 5537-5542.

This is the accepted version of the paper.

This version of the publication may differ from the final published version. To cite this item please consult the publisher's version.

Permanent repository link: <https://openaccess.city.ac.uk/id/eprint/14834/>

Copyright and Reuse: Copyright and Moral Rights remain with the author(s) and/or copyright holders. Copies of full items can be used for personal research or study, educational, or not-for-profit purposes without prior permission or charge, unless otherwise indicated, provided that the authors, title and full bibliographic details are credited, a hyperlink and/or URL is given for the original metadata page and the content is not changed in any way. For full details of reuse please refer to [City Research Online policy](#).

Characterization of silica nanowires for optical sensing
C. Themistos, M. Rajarajan, B.M.A. Rahman and K.T.V. Grattan
City University, London EC1V 0HB, UK

Abstract

The optical properties of silica nanowires in a Mach-Zehnder-based optical sensor for detecting biomaterial specimens have been studied using the full vectorial H-field formulation of the finite element method. The variation of the propagation constant, power fraction in the composite nanowires with the variation of the nanowire size, specimen refractive index and wavelength are also presented here.

Introduction

Recently, several types of nanowires, either metallic [1] or drawn from bulk glasses [2], as well as chemically grown nanoribbons [3], have been successfully fabricated and used as building blocks in the future micro- nano-photonics applications [4] in many fields such as biosensing [5] and non-linear optics [6]. Further, the combination of nanotechnology, biology, chemistry and photonics explores new opportunities for the development of optical sensors with subwavelength or nanometer structures. Silica nanowires [7] offer several advantages over other types of nanowires since they are based on material used among the most important photonic and opto-electronic applications within the visible and the near-infrared ranges, with their optical properties well studied. The study of photonic device applications, based on nanotechnology remains challenging because of high precision requirements, and therefore rigorous and highly accurate numerical approaches are required. The Finite Element Method (FEM) has been established as one of the most efficient numerical tools for the analysis of several photonics devices. In the present work the full-vectorial **H**-field formulation of the FEM [8] has been used for the study of the optical properties of silica nanowires in a Mach-Zehnder-based [9] optical sensor.

Results

The proposed Mach-Zehnder-based sensor system, formed by two uniform silica nanowires, one used as a reference arm and the other as a sensing arm with a certain length of a sensitive area, is presented in Fig.1(a). Both arms are immersed in aqueous solution and the surface of the sensing arm can be silanized and bio-modified with specific receptors and a thin layer around the wire is formed by the specimen under detection collected, as shown in the cross section of the composite waveguide in Fig.1(b).

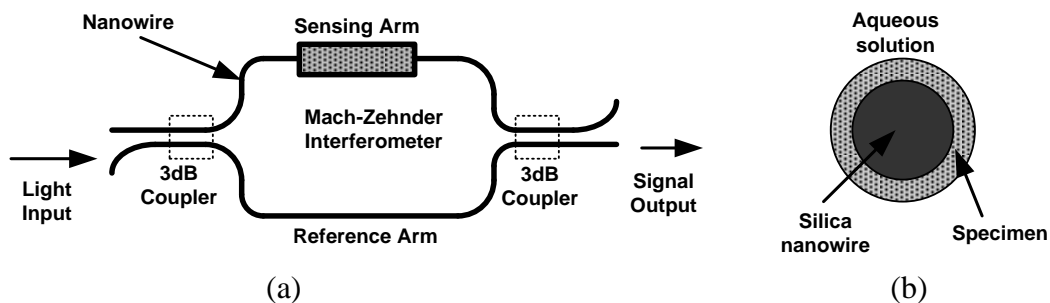


Fig.1 Schematic diagram of (a) the proposed sensor and (b) the cross section view of the composite waveguide, with a specimen layer.

A probing light that is launched through the nanowire propagates through the first 3dB coupler, operating as an optical splitter, is divided between the sensing and the reference arm and finally recombines via the second 3dB coupler, working as an optical combiner, as shown in Fig.1(a). The phase shift caused by the index change due to the specimen added in the sensing arm is numerically calculated and evaluated from the signal output of the lower nanowire, as presented in Figure 1(a).

Initially, the optical properties of the reference and the sensing arm of the single mode silica nanowires immersed in aqueous solution, where the latter is coated with the specimen under detection have been examined and the 3-D optical field profile of the H_x^{11} mode of the two arms, for a core, D , of 150nm and 700nm are presented in Fig.2.

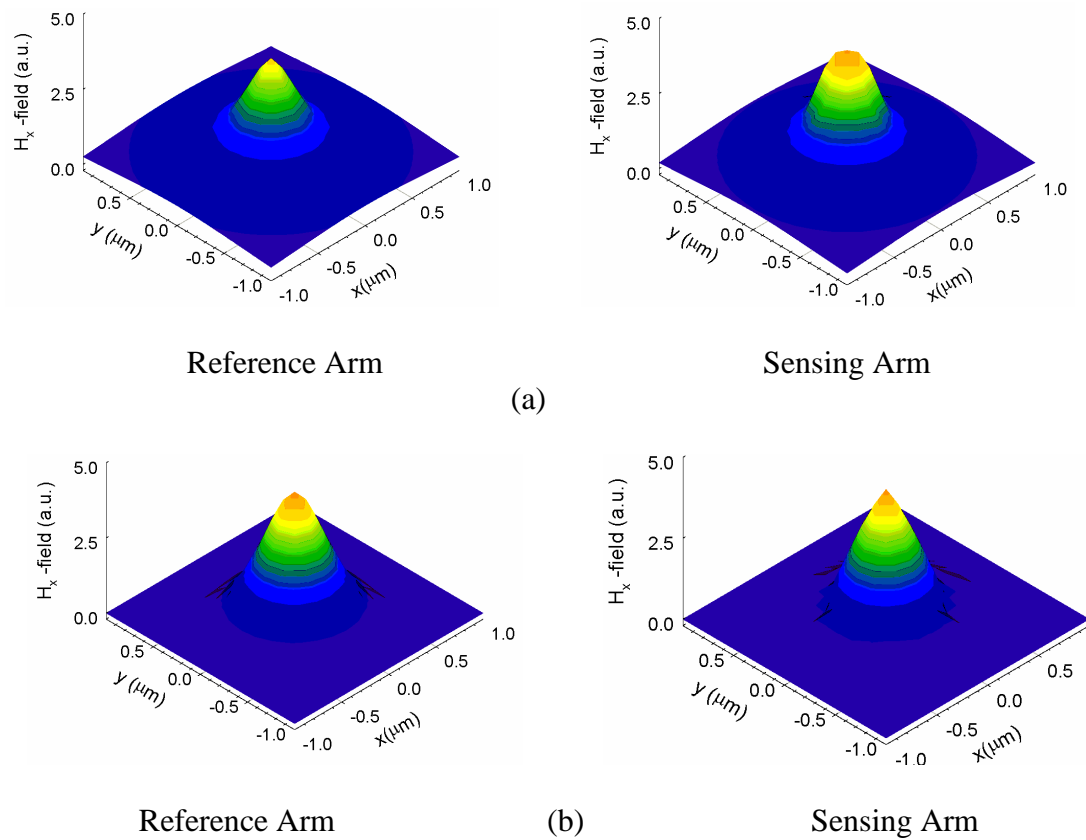


Fig.2 3-D field profile of the H_x^{11} mode for the reference and the sensing arm for (a) $D=150\text{nm}$ (b) $D=700\text{nm}$

The refractive index of the single mode silica nanowire and the aqueous solution (water) were considered to be 1.482 and 1.355, respectively, at an operating wavelength of 325 nm [10, 11]. The specimen thickness was assumed to be nanoparticles of 12 nm thickness with a refractive index value of 1.4 (polystreptavidin) [9]. As can be seen from the field profiles of the H_x^{11} optical mode for a core diameter, D , of 150 nm, shown in Fig.2 (a), the optical field is more confined in the reference arm, while for a core diameter of 700 nm the field confinement is found to be about the same for both arms, as presented in Fig.2 (b). [Can we state the spotsizes here for the two D 's?]As can be concluded from this figure, for a core diameter of 700 nm the mode is well confined and the sensing medium does not have much effect on the field

profile. However for a small core diameter of 150nm, a small change in the refractive index profile produces a larger change in the field profile.

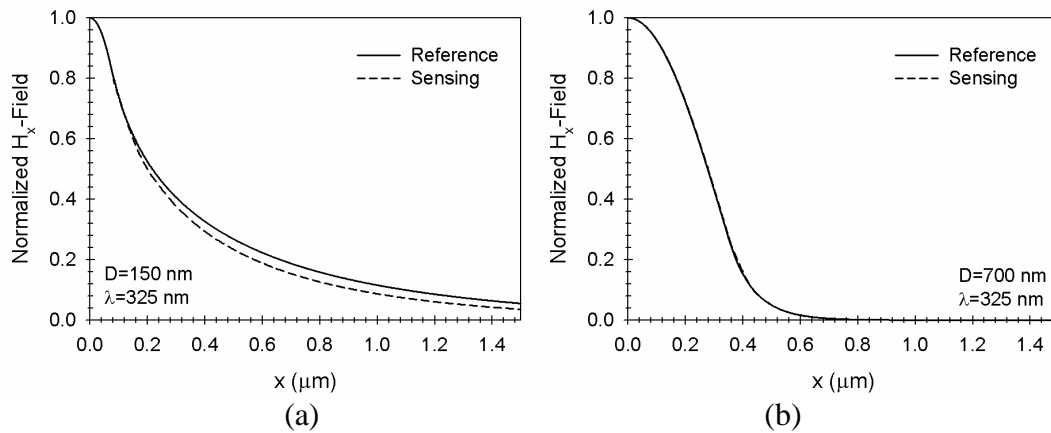


Fig.3 H_x along the x-axis for a fibre diameter of (a) $D=150$ nm (b) $D=700$ nm.

The optical field confinement in the reference and the sensing arm can be better viewed from the normalized H_x field profile along the horizontal (x)-axis, as presented in Fig.3(a) and Fig.3(b), for a nanowire core diameter of 150 nm and 700 nm, respectively. As can be seen from the above curves in Fig.3(b), the normalized optical fields for the reference and the sensing arm are almost identical for a core diameter, D , of 700 nm. However, when the core diameter, D , is 150nm a small variation in the optical field profile can be observed. Even for smaller d , field expands more outside, as it is operating closer to cutoff and hence influenced.

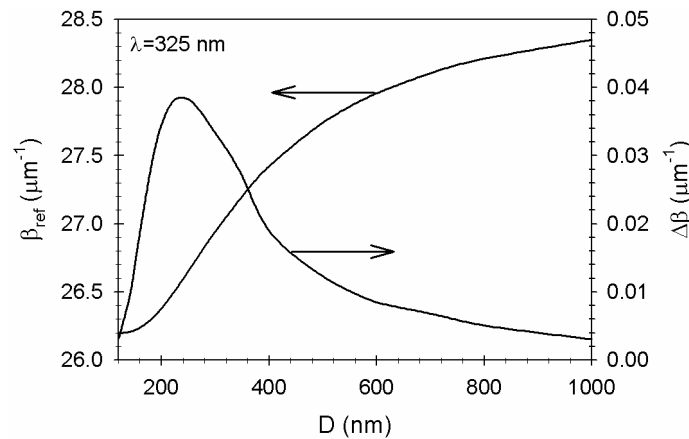


Fig.4 Propagation constant (reference arm) and propagation constant difference ($\Delta\beta$) (between reference and sensing arm) as a function of the fibre diameter (D).

Next, the variation of the propagation constant in the reference and the sensing arm with the silica nanowire diameter, D , has been examined and presented in Figure 4, where the propagation constant of the reference arm and the propagation constant difference between the two arms is plotted against a core diameter range from 100 nm to 1000 nm. As can be seen from the above characteristics as D decreased the propagation constant also reduces and the rate of reduction slowly increases. However, close to cutoff the propagation constant reduces at a lower rate. For a core diameter below 250 nm. The propagation constant difference, $\Delta\beta$, between the reference and the sensing arm, also presented in Figure 4, initially increases with the

increase of the core diameter. However, for a core diameter, D , of about 250 nm exhibits a peak value, and as the core diameter increases further this value reduces. A $75\mu\text{m}$ section can give π phase shift, necessary length for a sensor.

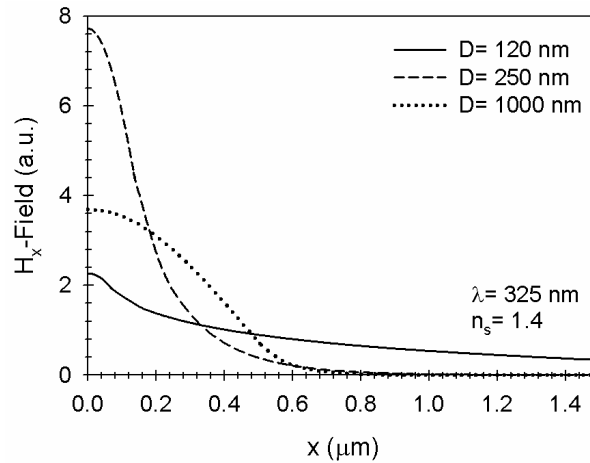


Fig.5 H_x field of the sensing arm for three different fibre diameters. $D=120, 250$ and 1000nm for a specimen index, $n_s=1.4$, **thickness??**

The axial H_x -field profile of the H_x^{11} optical mode for a core diameter of 120, 250 and 1000 nm has also been plotted in Fig.5, where it can be observed that for the smallest core diameter (120 nm) examined, the optical field not well confined in the core region and there exists appreciable amount of field intensity in the aqueous solution. The ratio of the boundary field intensity to the maximum field intensity, for a core diameter of $D=120, 250$ and 1000 nm, was calculated to be 0.89, 0.63 and 0.20, respectively. The ratio of the spot size area diameter to the core diameter was calculated to be 2.39, 0.87 and 0.55 nm, respectively, therefore it can be concluded that as the core diameter increases the optical field intensity becomes more confined within the core diameter. For a core diameter of 250 nm, near the core diameter at which the propagation constant difference between the reference and the sensing arm exhibits a peak value, as has been shown earlier in Fig.4, the optical field has the highest confinement, as shown in Fig.5. For the largest core diameter (1000 nm) examined, the optical confinement reduces but remains higher than the confinement for the smallest core diameter of 120 nm examined, as also presented in Fig.5.

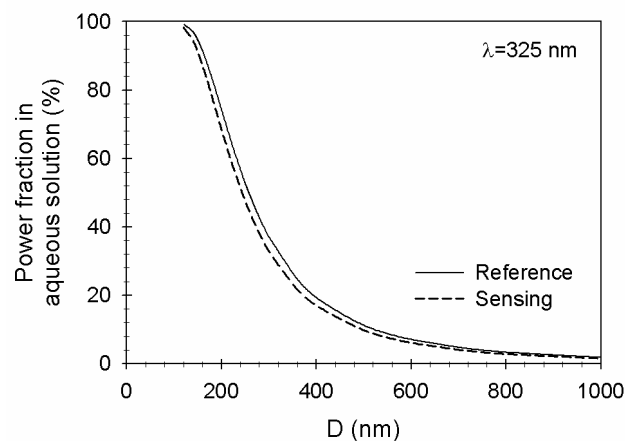


Fig 6 Power fraction in aqueous solution for the sensing and the reference arms as a function of the fibre diameter (D).

Further, the power fraction in the aqueous solution (water) for the reference and the sensing arm with the variation of the nanowire core diameter has also been studied and presented in Fig.6. As can be seen from the above characteristics, for a core radius of about $D=120$ nm, near the cutoff value of the optical mode the field extends mostly in the cladding (aqueous) region. For a core radius of about below 170 nm, more than 90% of the optical power in the aqueous solution, for both the reference and the sensing arm. As the value of D is increased further power in the aqueous solution is reduced since the field is more confined in the core region. However, for a a core radius of about $D=250$ nm, nearly 50% of the power is in the aqueous solution for both the reference and the sensing arms. It should be noted that at about this core radius, the propagation constant difference between the two arms exhibits a peak, as has been shown earlier in Fig.4. As can be seen from the above curves, the power fraction in the aqueous solution decreases in the both arms with the increase of the core diameter, with the power fraction in the sensing arm being slightly lower for the core diameter range examined.

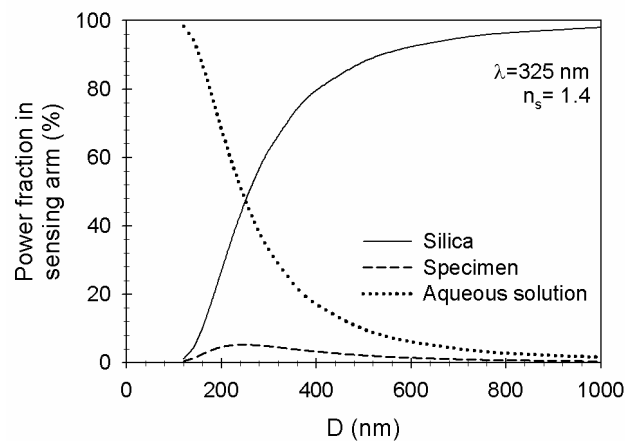
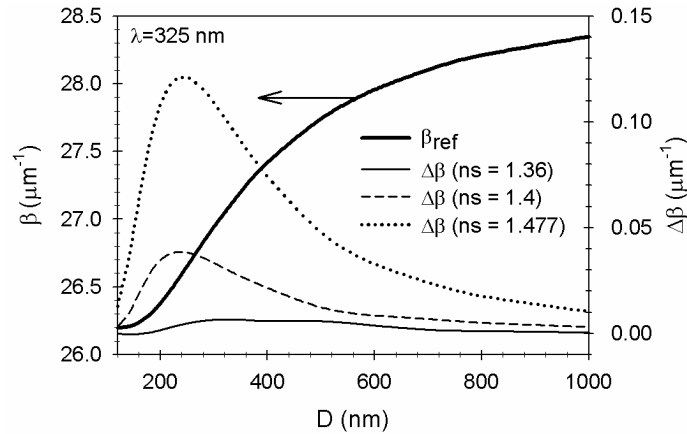


Figure 7 Power fraction of the sensing arm as a function of the fibre diameter for a specimen index, $n_s=1.4$

The power fraction in the different optical media of the sensing arm with the variation of the nanowire core diameter, for a specimen refractive index, n_s , of 1.4 has then been studied and presented in Fig.7. As can be seen from the above characteristics, for a small core diameter, the power fraction is minimum in the core and maximum in the specimen and aqueous solution regions. As the core diameter increases, the power fraction in the core and aqueous solution regions of the sensing arm revert and the power fraction in the core and the aqueous solution become maximum and minimum respectively, while the power in the specimen exhibits a peak near a core diameter of about 250 nm and above that decreases to zero.



make n_s (subscript) in the figure above

Fig.8 Change in propagation constant ($\Delta\beta$) as a function of the fibre diameter (D) for specimen indices of $n_s=1.35$, 1.4 and 1.477

Next, the variation of the propagation constant, β , and the propagation constant difference, $\Delta\beta$, (between the reference and the sensing arm) with the nanowire fibre diameter have been examined for different refractive index values and presented in Fig.8. The propagation constant of the reference arm increases with the increase of the fibre diameter, D, whereas the change in the propagation constant initially increases, reaching a peak value at a fibre diameter of about 250 nm and finally decreases for all the specimen refractive index values examined, as shown in Fig.8. From the above characteristics it can also be seen that for a specimen refractive index near the core refractive index the propagation constant difference, $\Delta\beta$, between the reference and the sensing arm is higher, compare to the propagation constant difference for the specimen with a refractive index near to the refractive index of the aqueous solution.

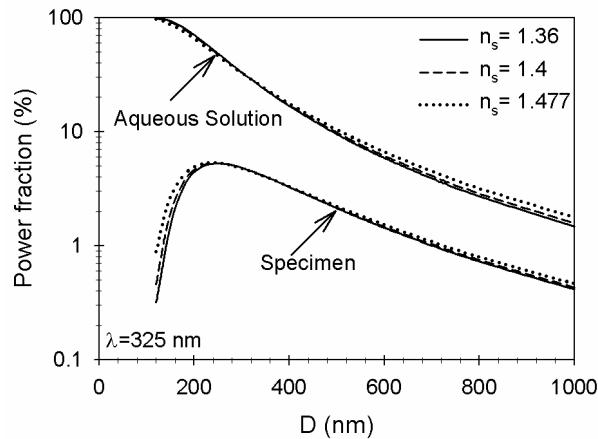


Fig. 9 Power fraction in the aqueous solution and specimen as a function of the fibre diameter (D) for specimen index of $n_s=1.36$, 1.4 and 1.477

Additionally, the power fraction in the specimen and the aqueous solution with the variation of the fibre diameter for different refractive indices of the specimen has been simulated and presented in Fig.9. As the value of D is reduced power in the silica region is slowly reducing and the power in the aqueous region is increasing. However, the power in the specimen initially increases and as the core thickness is increased further then the power is slowly reducing as near cutoff more power is in the aqueous solution. Hence an optimised design with maximum power in the specimen can

increase the sensitivity of the sensor. From the above curves it can be seen that the power fraction is always higher in the aqueous solution for all the range examined. The power in the aqueous solution decreases with the increase of the fibre diameter with the power fraction in the specimen with the lower refractive index being slightly higher for a larger fibre diameter. As can also be seen from the characteristics in Fig.9, the power fraction in the specimen increases with the fibre diameter, reaches a peak value at about 250 nm, following a decrease for larger fibre diameter, where the power fraction in the specimen with the lowest refractive index being slightly higher than in the other specimens examined. Increasing n_s slowly from 1.36 to 1.477 overall slows down the cutoff, which is clearly visible on this figure. However, due to the smaller thickness change the influence is very limited.

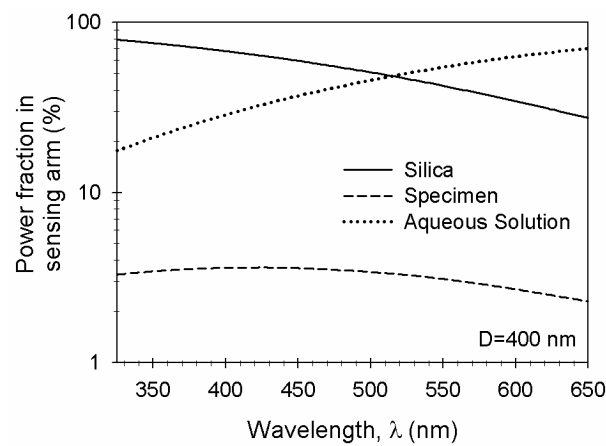


Fig.10 Power fraction for the sensing arm as a function of wavelength for a fibre diameter of $D=400\text{nm}$.

Finally, the change of the power fraction in the different regions of the sensing arm and the variation of the propagation constant difference between the reference and the sensing arm have been studied and presented in Fig.10 and Fig.11, respectively. As can be seen from the characteristics, shown in Fig.10, as the wavelength increases, the mode is weakly confined and hence less power in the core region and more power in the cladding aqueous region. The mode is well confined for smaller wavelength values and more power is in the core silica region. However, as the wavelength is increased the mode becomes weakly confined and more power is in the aqueous solution region compared to the silica core region.

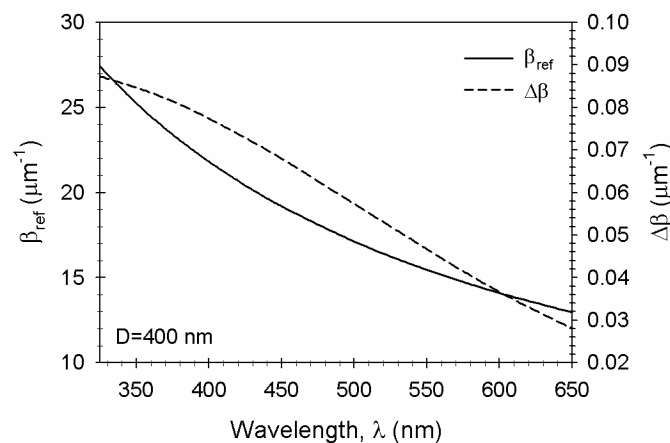


Fig.11 Change in propagation constant ($\Delta\beta$) and propagation constant as a function of the wavelength (λ)

The propagation constant of the reference arm and the propagation constant difference between the reference and the sensing arm, with the variation of the wavelength has been examined and presented in Fig.11. As can be seen from the above characteristics both curves decrease with the increase of the wavelength.

Fig 12. Effect of sample thickness varied from 12nm – 20nm? Can we do this Chris?

Conclusion

A rigorous finite element-based full vectorial H-field formulation has been used for the study of the optical properties of silica nanowires in a Mach-Zehnder-based optical sensor. The optical field profiles, the propagation constant difference and power fraction in the different regions of the reference and the sensing arm of the above device, studied thoroughly, in the present work are very important parameters in determining the sensitivity of the proposed optical sensors.

References

- [1] C. G. Poulton, M. A. Schmidt, G. J. Pearce, G. Kakarantzas, and P. St.J. Russell, "Numerical study of guided modes in arrays of metallic nanowires." *Opt. Lett.*, 32, pp.1647-1649, 2007.
- [2] L. Tong, L. Hu, J. Zhang, J. Qiu, Q. Yang, J. Lou, Y. Shen, J. He, and Z. Ye, "Photonic nanowires directly drawn from bulk glasses," *Opt. Express* 12, pp.82-87, 2006.
- [3] M. Law, D. J. Sirbully, J. C. Johnson, J. Goldberger, R. J. Saykally, and P. D. Yang, "Nanoribbon waveguides for subwavelength photonics integration," *Science* **305**, pp.1269-1273, 2004.
- [4] C. J. Barrelet, A. B. Greytak, and C. M. Lieber, "Nanowire photonic circuit elements," *Nano Lett.* **4**, 1981-1985, 2004.
- [5] P. Debackere, S. Scheerlinck, P. Bienstman, R. Baets, "Surface plasmon interferometer in silicon-on-insulator: novel concept for an integrated biosensor," *Opt. Express*, **14**, pp.7063-7072, 2006
- [6] M. A. Foster, A. C. Turner, M. Lipson, and A.L. Gaeta, "Nonlinear optics in photonic nanowires,"
- [7] L. Tong, R. R. Gattass, J. B. Ashcom, S. He, J. Lou, M. Shen, I. Maxwell, and E. Mazur, "Subwavelengthdiameter silica wires for low-loss optical wave guiding," *Nature* **426**, pp.816-819 2003.
- [8] B.M.A. Rahman and J.B. Davies, "Finite-element solution of integrated optical waveguides," *J. Lightwave Technol.*, **LT-2**, pp. 682-688, 1984.
- [9] B. J. Luff, J. S. Wilkinson, J. Piehler, U. Hollenbach, J. Ingenhoff, and N. Fabricius, "Integrated optical Mach-Zehnder biosensor," *J. Lightwave Technol.* **16**, 583-592 (1998).
- [10] P. Klocek, "*Handbook of Infrared Optical Materials*," Marcel Dekker, New York, 1991.
- [11] P. Schiebener, J. Straub, J. M. H. Levelt Sengers, and J. S. Gallagher, "Refractive index of water and steam as function of wavelength, temperature and density," *J. Phys. Chem. Ref. Data* **19**, pp.677-717, 1990.

